Int. J. Electrochem. Sci., 8 **(2013)** 4850 - 4863

International Journal of
ELECTROCHEMICAL
SCIENCE
www.electrochemsci.org

Electrochemical Characteristics of Layered-Spinel $0.7Li_2MnO_3 \cdot 0.3Li_4Mn_5O_{12}$ Composite Powders with Spherical Shape and Porous Nanostructure

Chul Min Sim, Jung Hyun Kim, Young Jun Hong, Jung-Kul Lee, Yun Chan Kang[*]

Department of Chemical Engineering, Konkuk University, 1 Hwayang-dong, Gwangjin-gu, Seoul 143-701, Korea
*E-mail: yckang@konkuk.ac.kr

Received: 4 February 2013 / *Accepted:* 27 February 2013 / *Published:* 1 April 2013

Layered-spinel $0.7Li_2MnO_3 \cdot 0.3Li_4Mn_5O_{12}$ composite cathode powders are prepared by spray pyrolysis. Composite powders post-treated at temperatures below 800°C have spherical shapes and porous nanostructures. The BET surface areas of the composite powders decrease from 18.8 to 1.8 $m^2 g^{-1}$ when the post-treatment temperature is increased from 550°C to 850°C. The composite powders post-treated at temperatures below 700°C have similar charge capacities due to the $Mn^{3+/4+}$ redox reaction of the spinel component when they are initially charged to 4.5 V (about 41 mAh g^{-1}). However, the initial charge capacities of the composite powders post-treated at 550°C, 600°C, 650°C, and 700°C are 203, 197, 166, and 105 mAh g^{-1}, respectively, when they are charged to 4.95 V. The elimination of Li_2O from the layered Li_2MnO_3 component is affected by the crystallite size of the Li_2MnO_3 phase as well as the grain size in the composite powders. The discharge capacities of the composite powders post-treated at 600°C increase from 220 to 263 mAh g^{-1} after 3 cycles. Then, the discharge capacities monotonically decrease to 201 mAh g^{-1} after 30 cycles.

Keywords: composite material; cathode material; spray pyrolysis; lithium battery

1. INTRODUCTION

It is well known that Li-Mn spinel is one of the most promising candidates for the cathode material of lithium secondary batteries [1,2]. Li-Mn spinel has significant advantages, such as low cost, abundance, safety, ease of preparation, and nontoxicity. However, since its capacity fades during cycling, particularly at elevated temperatures and high voltages, its application has been limited. However, the upper cutoff voltage limit has been gradually increased in an attempt to increase the reversible capacity of this cathode material.

Lithium-rich layered-layered composite materials have high charge/discharge capacities when they are electrochemically activated at approximately 4.6 V [3-21]. Johnson et al. prepared layered-spinel composite cathode powders using the solid-state reaction method [22]. When these layered-spinel composite cathode powders were cycled between 5 and 2 V, a rechargeable capacity >250 mAh g^{-1} was achieved [22]. The characteristics of the layered-layered composite cathode materials are strongly affected by the process adopted for preparing the powders [12-17]. The solid-state reaction method does not produce composite powders with a uniform composition. Liquid solution methods, including the coprecipitation, sol-gel, and sucrose combustion methods, have been applied to prepare layered-layered composite cathode powders [17-21]. However, layered-spinel composite cathode materials have scarcely been studied in the field of advanced ceramic manufacturing processes.

In this study, layered-spinel $0.7Li_2MnO_3 \cdot 0.3Li_4Mn_5O_{12}$ composite cathode powders were prepared by spray pyrolysis. Spinel $Li_4Mn_5O_{12}$ has previously been proposed and studied as a promising positive electrode material for lithium secondary batteries [23-25]. $Li_4Mn_5O_{12}$ cathode material prepared by conventional methods had an initial discharge capacity of about 140 mAh g^{-1} in the range of cell voltages from 2.5 to 3.6 V [23]. Spray pyrolysis, a gas-phase reaction method, is advantageous for the preparation of multicomponent, nonaggregated cathode powders [26-31]. The morphological and electrochemical properties of the $0.7Li_2MnO_3 \cdot 0.3Li_4Mn_5O_{12}$ composite powders post-treated at various temperatures were investigated.

2. EXPERIMENTAL

The spray pyrolysis equipment consists of three parts: a six-pack ultrasonic spray generator operated at 1.7 MHz, a 1000-mm-long tubular quartz reactor of 50-mm ID, and a bag filter for collecting particles. The precursor solution was prepared by dissolving stoichiometric amounts of lithium nitrate (98%, Junsei) and manganese nitrate hexahydrate (97%, Junsei) in distilled water. The overall concentration of the Li and Mn components in the solution was 0.5 M. The powders were obtained by spray pyrolysis at 900°C. The flow rate of air used as the carrier gas was fixed at 20 L min^{-1}. The as-prepared powders were post-treated in a box furnace at various temperatures ranging from 550°C to 850°C for 3 h in air atmosphere.

The crystal structures of the prepared cathode powders were investigated using X-ray diffractometry (XRD; RIGAKU DMAX-33) with Cu Kα radiation (λ = 1.5418 Å). The morphological characteristics of the powders were investigated using scanning electron microscopy (SEM; JEOL, JSM-6060) and transmission electron microscopy (TEM, JEOL, JEM-2100F). The specific surface areas of the composite cathode powders were measured using the Brunauer-Emmett-Teller (BET) method. The capacities and cycle properties of the powders were determined by using a 2032-type coin cell. The cathode electrode was prepared from a mixture containing 20 mg of $0.7Li_2MnO_3 \cdot 0.3Li_4Mn_5O_{12}$ and 12 mg of TAB (TAB is a mixture of 9.6 mg of teflonized acetylene black and 2.4 mg of a binder). Lithium metal and microporous polypropylene film were used as the counter electrode and separator, respectively. The electrolyte was 1 M $LiPF_6$ in a 1:1 mixture by volume of ethylene carbonate (EC)/dimethyl carbonate (DMC). The cell was assembled in a glove box

in an argon atmosphere. The charge/discharge characteristics of the samples were measured by cycling in the potential range of 2–4.95 V at 23 mA g^{-1}. Cyclic voltammetry (CV) was performed for the potential interval of 2.0–4.95 V vs. Li^+/Li.

3. RESULTS AND DISCUSSION

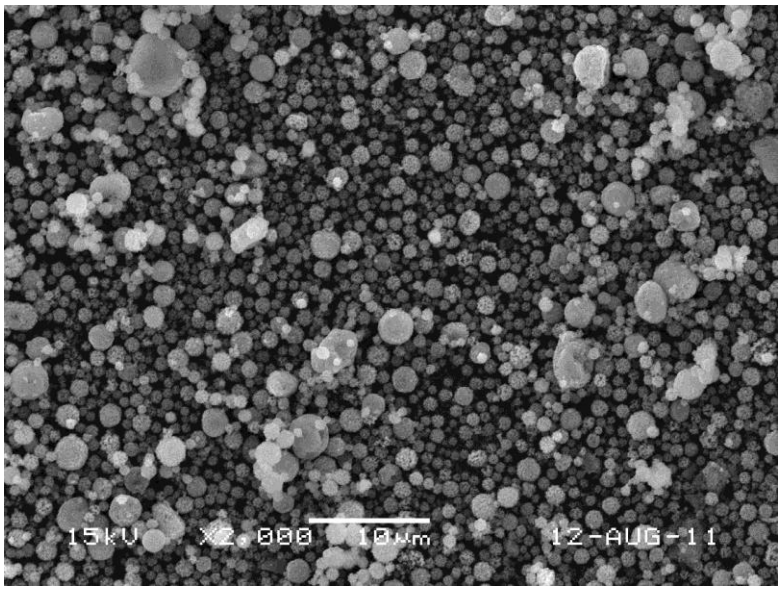

(a)

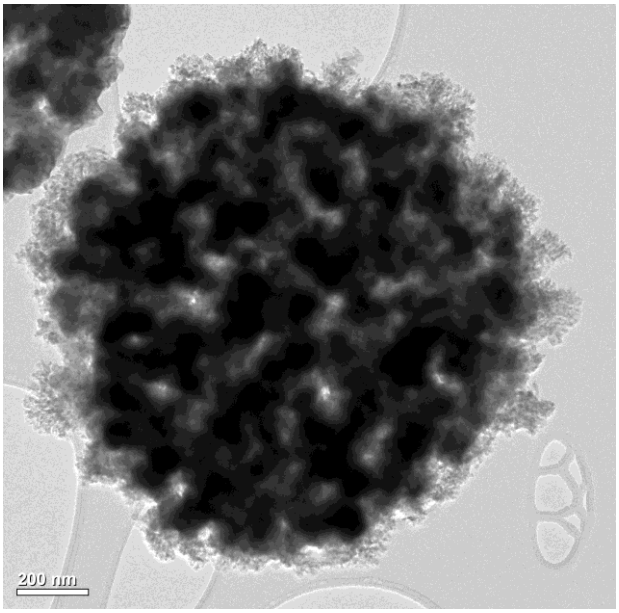

(b)

Figure 1. SEM and TEM images of the $0.7Li_2MnO_3$-$0.3Li_4Mn_5O_{12}$ precursor powders prepared by spray pyrolysis.

The morphology of the precursor powders obtained by spray pyrolysis is shown in Fig. 1. The precursor powders had aggregated structures of primary particles, spherical shapes, and submicron

sizes. The sizes of the primary particles in the TEM image were as fine as several nanometers because of the short residence time, 4 s, of the powders inside the hot wall reactor. The precursor powders were post-treated to improve the physical and electrochemical properties of the cathode powders. The XRD patterns of the precursor powders and the powders post-treated at various temperatures are shown in Fig. 2.

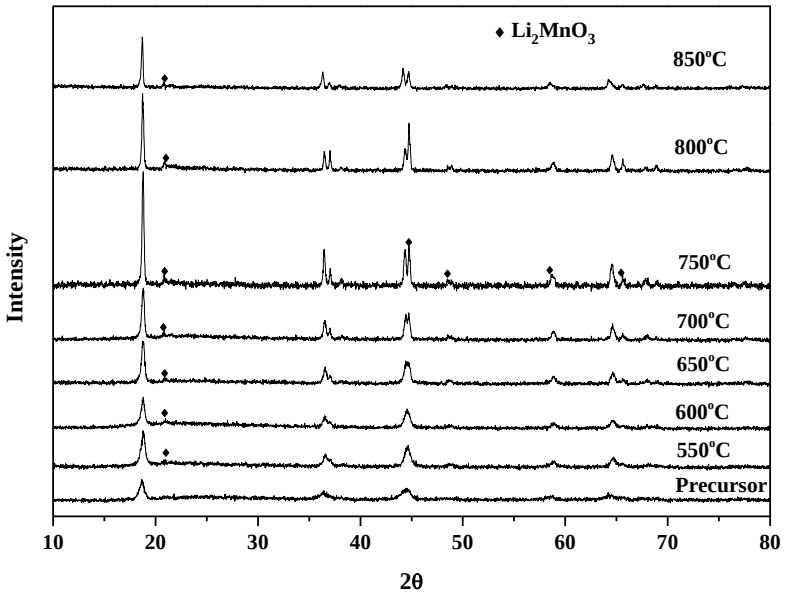

Figure 2. XRD patterns of the $0.7Li_2MnO_3$-$0.3Li_4Mn_5O_{12}$ composite powders post-treated at various temperatures.

The XRD pattern of the precursor powders indicated a crystal structure similar to those of the post-treated powders, even for such a short residence time of the powders inside the hot wall reactor. However, the precursor powders had highly disordered structures, judging from the broadened peaks. The peaks of the XRD patterns sharpened when the post-treatment temperature increased from 550°C to 750°C. The post-treated powders had a superlattice peak near 21° that can be attributed to the superlattice structure of the layered Li_2MnO_3 [3-5]. Therefore, the post-treated powders had a layered-spinel composite structure. The intensity of the layered Li_2MnO_3 peak appearing near 21° increased with increasing post-treatment temperature up to 800°C. The layered Li_2MnO_3 phase in composite powders has previously been reported to be stable at post-treatment temperatures below 750°C [22]. In this study, the decomposition of the layered Li_2MnO_3 phase occurred at 850°C, beyond which the peak intensity of the layered Li_2MnO_3 phase strictly decreased. The intensity of the spinel peak appearing near 45° increased with increasing post-treatment temperature up to 750°C. The decomposition of the spinel phase occurred at 800°C. Therefore, the intensities of the XRD peaks of the composite powders decreased at temperatures above 800°C. Clear separation of the XRD peaks of the spinel and the layered phases near 45° was observed at high post-treatment temperatures above 700°C.

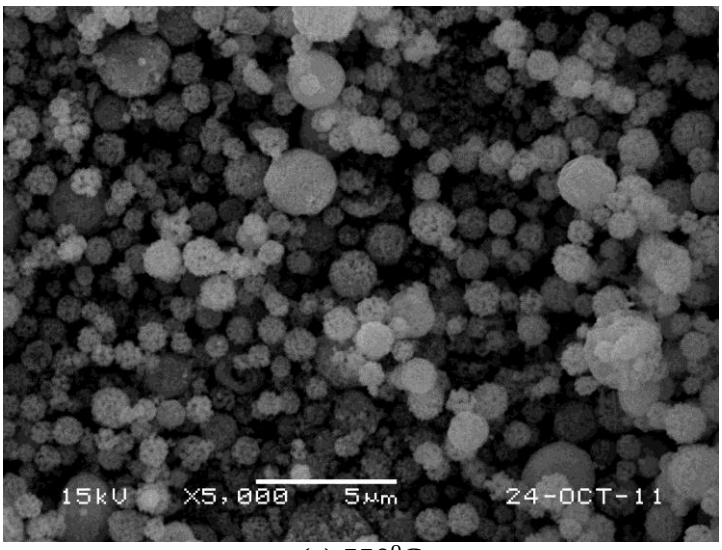

(a) 550°C

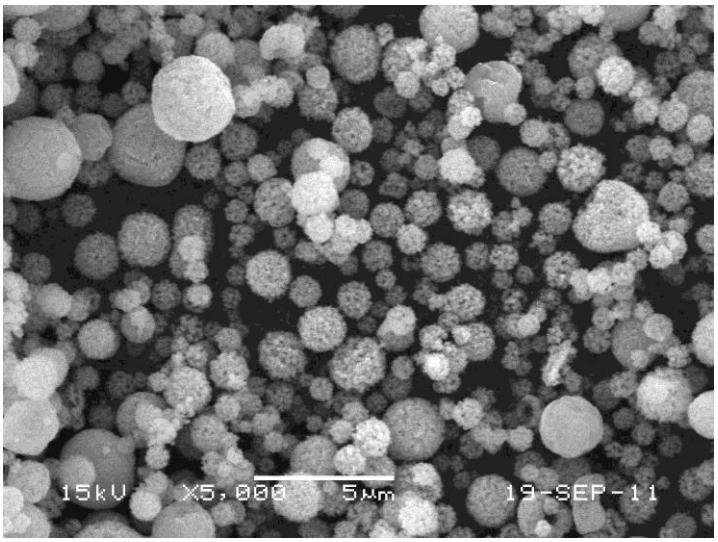

(b) 600°C

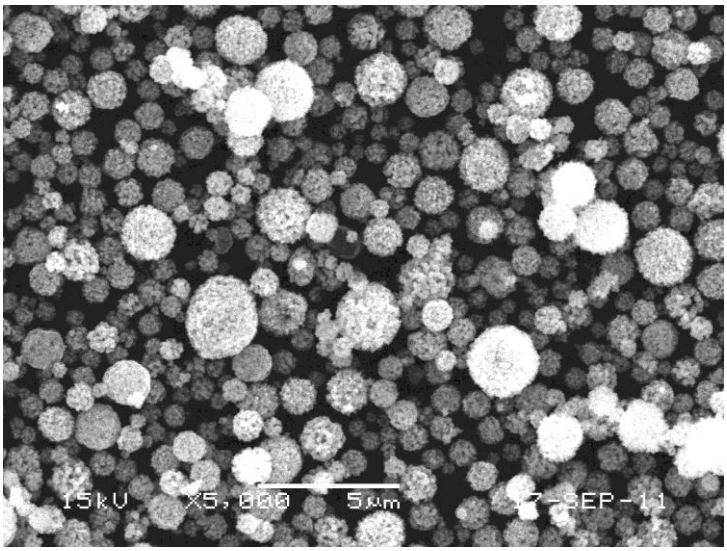

(c) 650°C

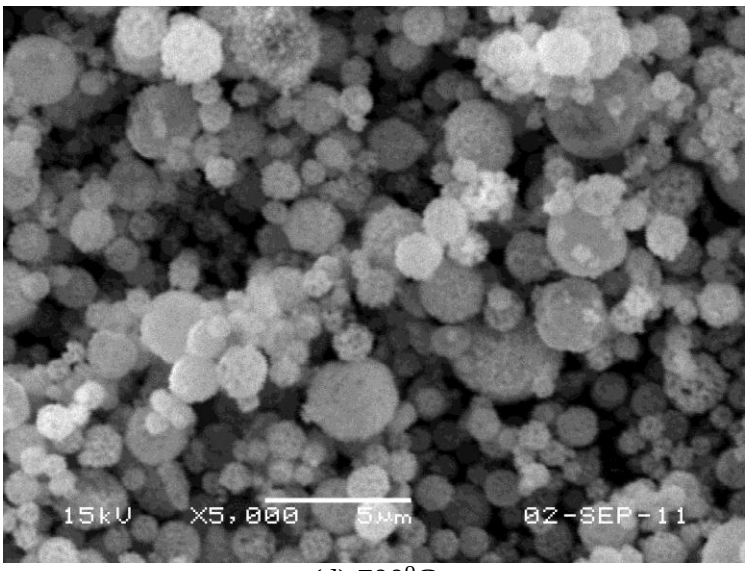

(d) 700°C

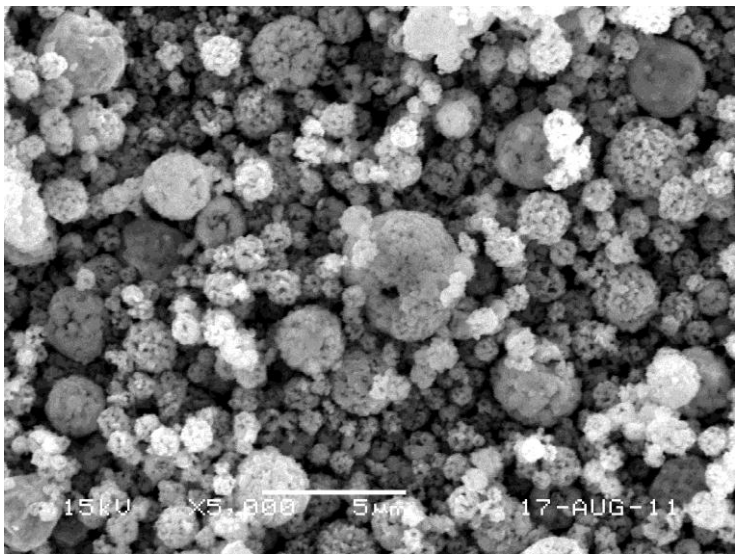

(e) 750°C

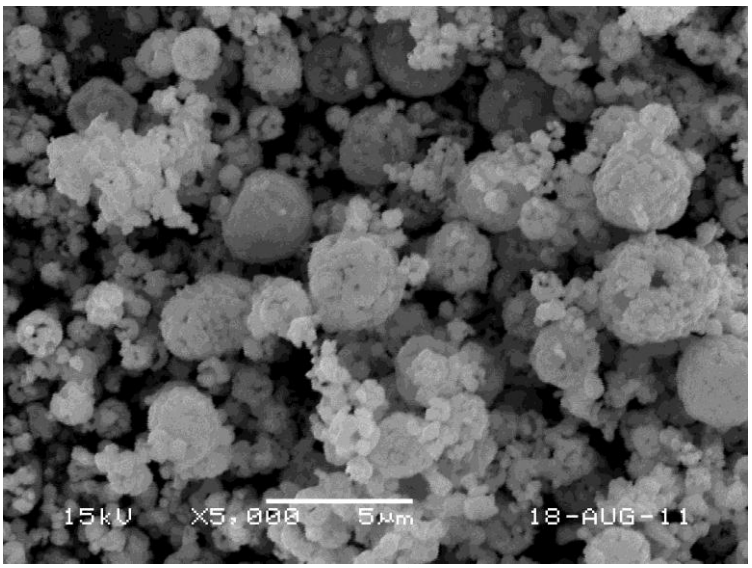

(f) 800°C

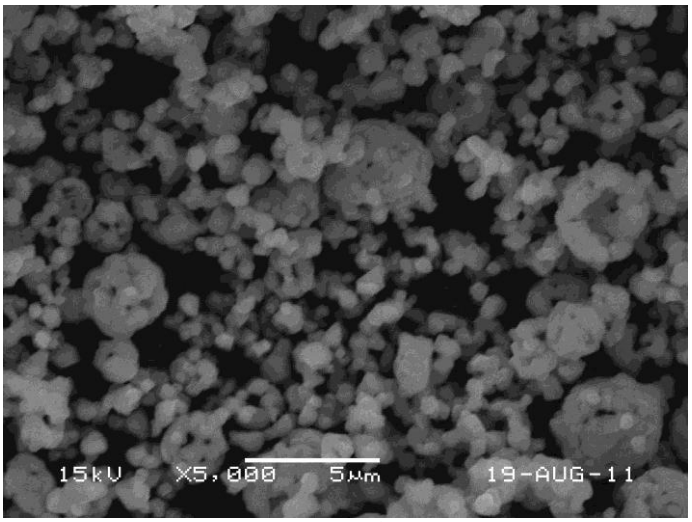

(g) 850°C

Figure 3. SEM images of the $0.7Li_2MnO_3$-$0.3Li_4Mn_5O_{12}$ composite powders post-treated at various temperatures.

Fig. 3 shows the morphologies of the post-treated $0.7Li_2MnO_3 \cdot 0.3Li_4Mn_5O_{12}$ composite powders. The composite powders post-treated at temperatures below 750°C had spherically shaped particles and aggregated nanostructures. However, grain growth in the composite powders above 800°C destroyed the spherical shapes of the precursor powder particles. The BET surface areas of the precursor powder and the composite powder post-treated at 600°C were 20.7 and 16.7 $m^2\ g^{-1}$, respectively. The post-treatment of the composite powders at 600°C slightly decreased the BET surface area through crystal growth. When the two solid phases are mixed, each phase prevents the crystal growth of the other phase. Therefore, the composite powders had fine grain sizes and high surface areas even after post-treatment at 600°C for 3 h. However, the BET surface areas of the composite powders post-treated at 750°C, 800°C, and 850°C were 6.2, 3.4, and 1.8 $m^2\ g^{-1}$, respectively.

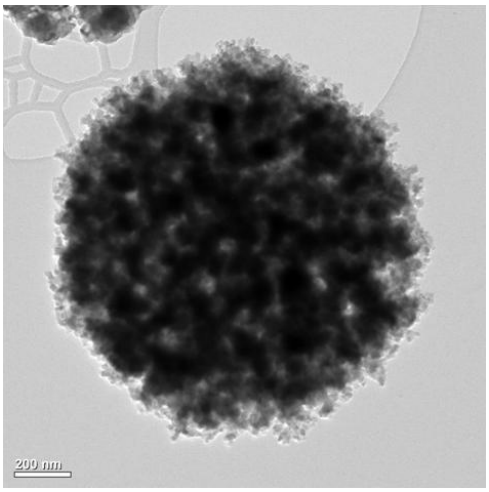

(a)

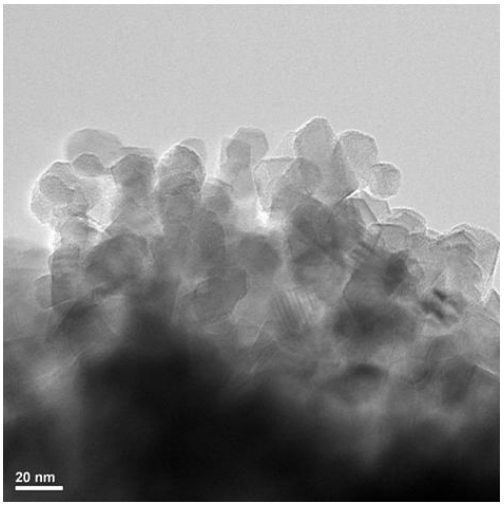

(b)

Figure 4. TEM images of the $0.7Li_2MnO_3$-$0.3Li_4Mn_5O_{12}$ composite powders post-treated at 600°C.

Abrupt grain growth of the composite powders occurred at a post-treatment temperature of 800°C. Fig. 4 shows low- and high-resolution TEM images of the $0.7Li_2MnO_3$-$0.3Li_4Mn_5O_{12}$ composite powders post-treated 600°C. The mean size of the primary particles measured from the TEM image was 17 nm.

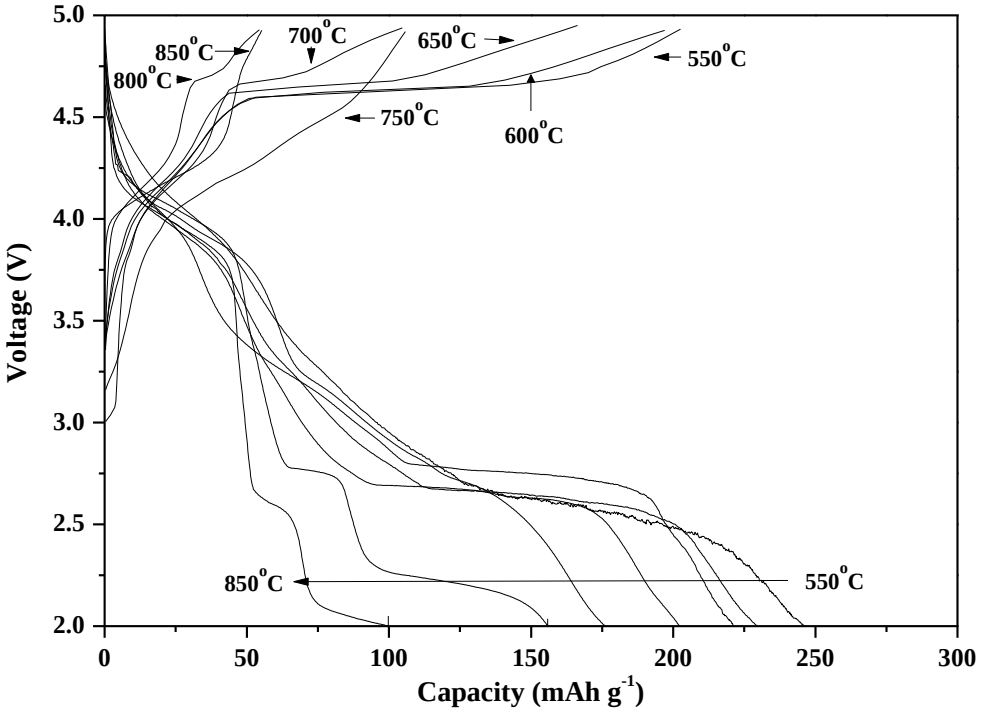

Figure 5. Initial charge-discharge curves of $0.7Li_2MnO_3$-$0.3Li_4Mn_5O_{12}$ composite powders post-treated at various temperatures.

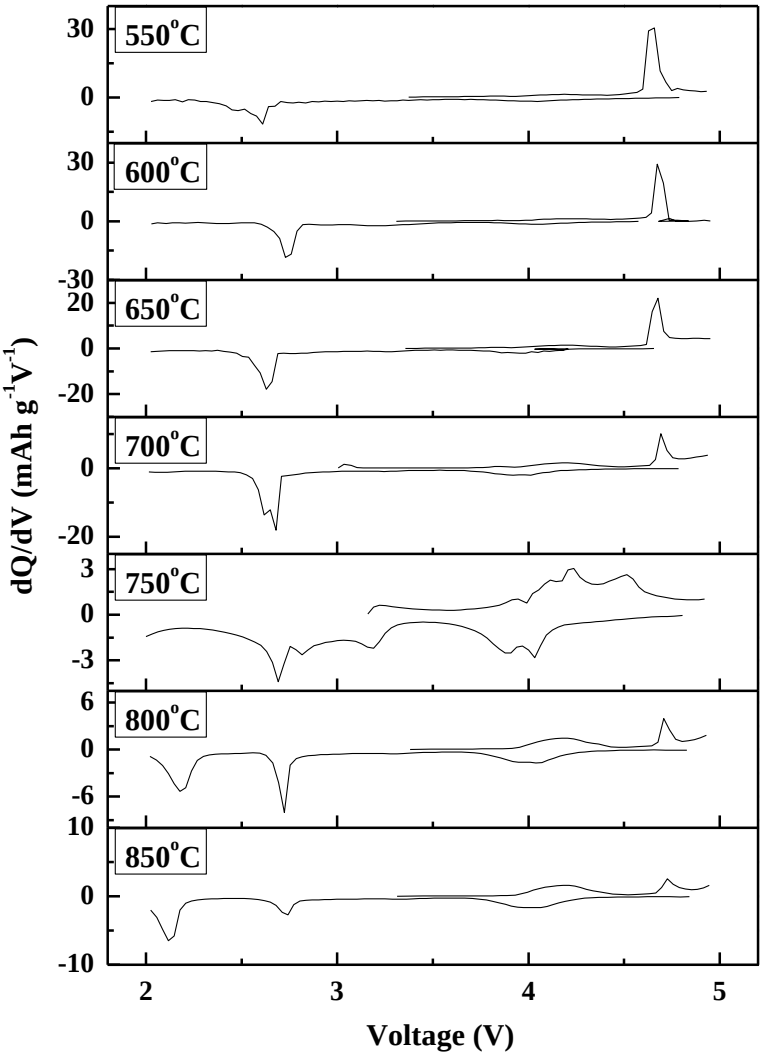

Figure 6. *dQ/dV* versus *V* curves of the initial cycles for $0.7Li_2MnO_3$-$0.3Li_4Mn_5O_{12}$ composite powders post-treated at various temperatures.

Figs. 5 and 6 show the initial charge-discharge curves and the differential capacity vs. voltage (*dQ/dV*) curves of Li/$0.7Li_2MnO_3$-$0.3Li_4Mn_5O_{12}$ electrodes post-treated at various temperatures. The initial charge and discharge curves showed the characteristics of the layered and spinel composite powders irrespective of the post-treatment temperature. However, the initial charge and discharge capacities due to the layered and spinel phases of the composite powders were different for different post-treatment temperatures. The composite powders post-treated at temperatures below 700°C had similar charge capacities due to the $Mn^{3+/4+}$ redox reaction of the spinel component when they were initially charged to 4.5 V (about 41 mAh g^{-1}). The small charge capacities of the composite powders below 4.5 V for all post-treatment temperatures indicate that a small amount of Mn^{3+} exists in the composite powders. However, the initial charge capacities of the composite powders decreased from 203 to 105 mAh g^{-1} when the post-treatment temperature increased from 550 to 700°C (see table 1).

Table 1. Initial charge and discharge capacities, and first cycle efficiencies of the composite powders post-treated at various temperatures.

	Charge capacity (mAh g^{-1})	Discharge capacity (mAh g^{-1})	First cycle efficiency (%)
550°C	203	244	120
600°C	197	228	116
650°C	166	220	132
700°C	105	201	191
750°C	106	176	166
800°C	54	133	246
850°C	64	99	155

The voltage plateau in the initial charge curves near 4.7 V was attributed to the removal of Li_2O from the layered Li_2MnO_3 component [7,8]. The intensity of the oxidation peak near 4.7 V due to the removal of Li_2O from the layered Li_2MnO_3 component of the composite powders decreased with increasing the post-treatment temperature, as shown in the *dQ/dV* curves in Fig. 6. The charge capacities of the composite powders post-treated at 550°C, 600°C, 650°C, and 700°C delivered by the layered Li_2MnO_3 component were 107, 79, 57, and 22 mAh g^{-1}, respectively. The sharpness of the XRD peaks of the layered Li_2MnO_3 component of the composite powders increased with increasing post-treatment temperature up to 750°C, as shown in the XRD patterns. In addition, the spinel $Li_4Mn_5O_{12}$ component can gradually decompose to the spinel $LiMn_2O_4$ and the layered $LiMnO_2$ and Li_2MnO_3 components at high post-treatment temperatures above 600°C [24,32]. Therefore, the relative abundance of the layered Li_2MnO_3 component in the composite powders will increase with increasing post-treatment temperature. However, the charge capacities of the composite powders delivered by the layered Li_2MnO_3 component decreased with increasing post-treatment temperature. The elimination of Li_2O from the layered Li_2MnO_3 component was affected by the crystallite size of the Li_2MnO_3 phase as well as the grain size in the composite powders. The crystal growth in the composite powders at higher post-treatment temperatures inhibited the formation of the MnO_2 component from Li_2MnO_3 by elimination of Li_2O in the first charging process. The composite powders post-treated at temperatures of 750°C and 800°C had larger initial charge capacities (>70 mAh g^{-1}) due to the $Mn^{3+/4+}$ redox reaction than did the composite powders post-treated at temperatures below 700°C when they were initially charged to 4.5 V. The formation of electrochemically active spinel $LiMn_2O_4$ and layered $LiMnO_2$ components increased the initial charge capacities in the low-voltage region. On the other hand, the voltage plateau above 4.5 V, which was attributed to the removal of Li_2O from the layered Li_2MnO_3 component, was not observed in the initial charge curves of the composite powders post-treated at temperatures of 750 and 800°C. The abrupt growth of the Li_2MnO_3 crystals and the grains of the composite powders post-treated at 750°C and 800°C, as shown in the XRD patterns and the SEM images, reduced the amount of elimination of Li_2O from the layered Li_2MnO_3 component. The low initial charge capacity of the composite powders post-treated at 850°C when they were charged to 4.95 V is due to the decomposition of the layered and the spinel Li-Mn-O components. The peak intensities in the XRD pattern abruptly decreased at a post-treatment temperature of 850°C. The initial discharge

capacities of the composite powders decreased from 244 to 99 mAh g^{-1} when the post-treatment temperature increased from 550 to 850°C.

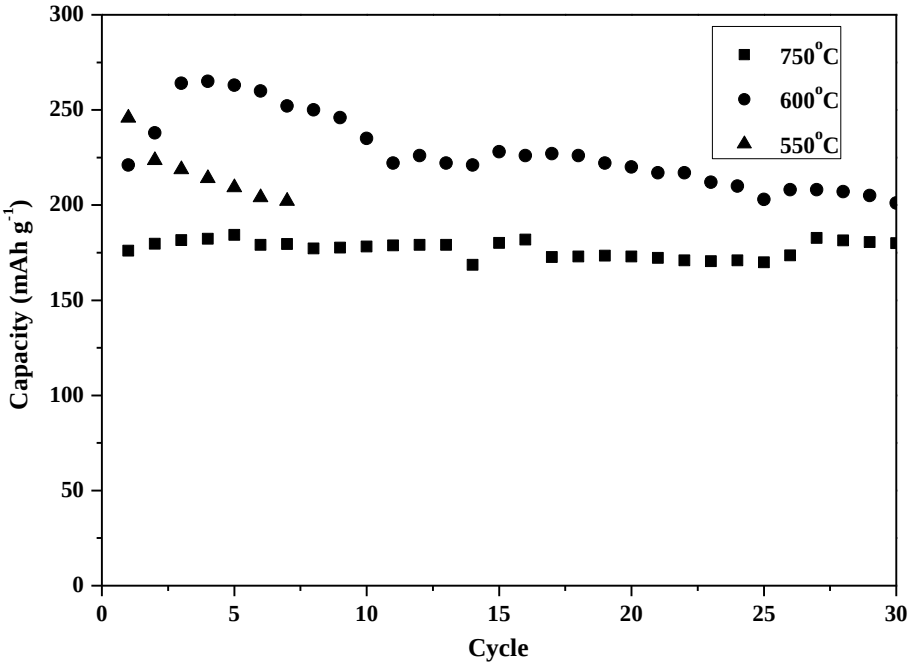

Figure 7. Cycling performances of $0.7Li_2MnO_3$-$0.3Li_4Mn_5O_{12}$ composite powders post-treated at various temperatures.

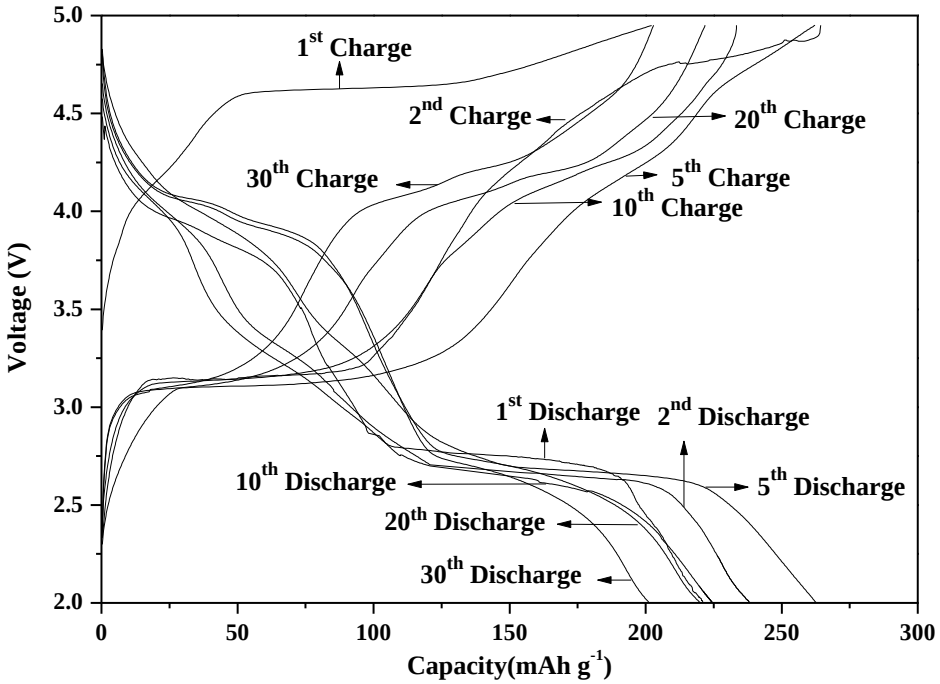

Figure 8. The charge-discharge curve profiles of 1st, 2nd, 5th, 10th, 20th, and 30th cycles for $0.7Li_2MnO_3$-$0.3Li_4Mn_5O_{12}$ composite powders post-treated at 600°C.

Fig. 7 shows the cycle properties of the layered-spinel composite cathode powders. The discharge capacity of the composite powders post-treated at 550°C abruptly decreased from 245 to 202 mAh g^{-1} after 7 cycles. The composite powders post-treated at 550°C had a large amount of the layered Li_2MnO_3 component, as shown in the initial charge and *dQ/dV* curves in Figs. 5 and 6. However, the Li_2MnO_3 component of the composite powders post-treated at 550°C was easily electrochemically activated because of fine crystallites dispersed in the nanostructured composite powders with a high surface area.

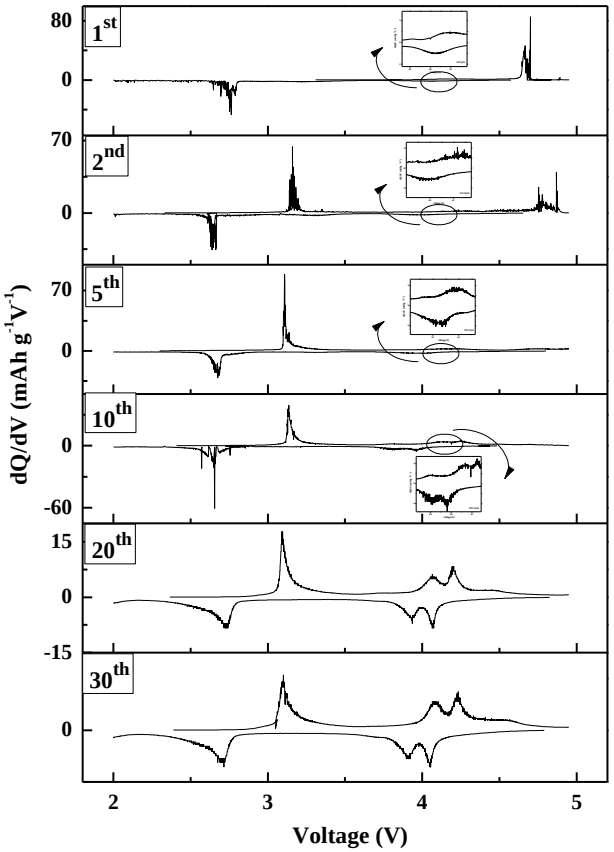

Figure 9. *dQ/dV* versus *V* curves of 1st, 2nd, 5th, 10th, 20th, and 30th cycles for $0.7Li_2MnO_3$-$0.3Li_4Mn_5O_{12}$ composite powders post-treated at 600°C.

A high percentage of the Li_2MnO_3 component was changed into a spinel component through the MnO_2 component in the initial charging and discharging processes. Therefore, the structural stability provided by the Li_2MnO_3 component was not observed in the cycle properties of the composite powders post-treated at 550°C. The discharge capacities of the composite powders post-treated at 750°C were initially low, 176 mAh g^{-1}. However, the composite powders post-treated at a high temperature of 750°C had good cycle properties because of the structural stability provided by the Li_2MnO_3 component, even at a high operation voltage [22]. The discharge capacities of the composite powders post-treated at 600°C increased from 221 to 264 mAh g^{-1} after 3 cycles. Then, the discharge

capacities monotonically decreased to 201 mAh g^{-1} after 30 cycles. Figs. 8 and 9 show the charge/discharge and *dQ/dV* curves of the composite powders post-treated at 600°C after various numbers of cycles. The clear voltage plateau near 4.7 V was also observed in the charge curve of the second cycle, as shown in Fig. 8. MnO_2 material was formed from Li_2MnO_3 by elimination of Li_2O in the first several charging processes. The oxidation peak near 4.7 V was also observed in the *dQ/dV* curve of the second cycle in Fig. 9. On the other hand, the oxidation peak near 4.7 V was not observed in the *dQ/dV* curve of the fifth cycle. Activation of the inactive MnO_2 component formed from Li_2MnO_3 into an active layered or spinel component increased the discharge capacities of the cathode powders within 3 cycles. The voltage plateaus near 4.0 V in the discharge curves become increasingly flatter with increasing cycle number in Fig. 8. The layered structure formed from the inactive MnO_2 slowly transformed into a spinel structure. The *dQ/dV* curves of the composite powders after the 30th cycle had the same shapes as that of pure spinel $LiMn_2O_4$ [33].

4. CONCLUSIONS

The physical and electrochemical properties of layered-spinel $0.7Li_2MnO_3{\cdot}0.3Li_4Mn_5O_{12}$ composite cathode powders prepared by spray pyrolysis were investigated. The prepared and post-treated composite powders had spherically shaped particles and porous nanostructures. Decomposition of the layered Li_2MnO_3 and spinel phases occurred at 850°C and 800°C, respectively. The initial charge capacities of the composite powders post-treated at 550°C, 600°C, 650°C, and 700°C were 203, 197, 166, and 105 mAh g^{-1}, respectively, when they were charged to 4.95 V. The relative abundance of the layered Li_2MnO_3 component in the composite powders increased with increasing post-treatment temperature up to 800°C. However, the initial charge capacities of the composite powders delivered by the layered Li_2MnO_3 component decreased with increasing post-treatment temperature. The crystal growth in the composite powders at higher post-treatment temperatures inhibited the formation of the MnO_2 component from Li_2MnO_3 by elimination of Li_2O in the first charging process. The discharge capacities of the composite powders post-treated at 600°C changed from 264 to 201 mAh g^{-1} after 30 cycles. The structural stability provided by the Li_2MnO_3 component improved the cycle properties of the composite cathode powders even at high operation voltage.

ACKNOWLEDGEMENT
This work was supported by the National Research Foundation of Korea (NRF) grant funded by the Korea government (MEST) (No. 2012R1A2A2A02046367). This research was supported by Basic Science Research Program through the National Research Foundation of Korea (NRF) funded by the Ministry of Education, Science and Technology (2012R1A1B3002382). This work was supported by Seoul R&BD Program (WR090671).

References

1. J.M. Tarascon, D. Guyomard, *Electrochim. Acta*, 38 (1993) 1221.

2. C.S. Johnson, *J. Power Sources*, 165 (2007) 559.
3. Z. Lu, L.Y. Beaulieu, A. Donaberger, C.L. Thomas, J.R. Dahn, *J. Electrochem. Soc*., 149 (2002) A778.
4. Z. Lu, Z. Chen, J.R. Dahn, *Chem. Mater*., 15 (2003) 3214.
5. M.M. Thackeray, S.H. Kang, C.S. Johnson, J.T. Vaughey, R. Benedek, S.A. Hackney, *J. Mater. Chem*., 17 (2007) 3112.
6. P.S. Whitfield, S. Niketic, I.J. Davidson, *J. Power Sources*, 146 (2005) 617.
7. C.S. Johnson, J.S. Kim, C. Lefief, N. Li, J.T. Vaughey, M.M. Thackeray, *Electrochem. Commun.*, 6 (2004) 1085.
8. S.H. Kang, P. Kempgens, S. Greenbaum, A.J. Kropf, K. Amine, M.M. Thackeray, *J. Mater. Chem.*, 17 (2007) 2069.
9. J.S. Kim, C.S. Johnson, J.T. Vaughey, M.M. Thackeray, *Chem. Mater*., 16 (2004) 1996.
10. M. Tabuchi, K. Tatsumi, S. Morimoto, S. Nasu, T. Saito. Y. Ikeda, *J. Appl. Apps*., 104 (2008) 043909.
11. M.M. Thackeray, C.S. Johnson, J.T. Vaughey, N. Li, S.A. Hackney, *J. Mater. Chem*., 15 (2005) 2257.
12. C. Storey, I. Kargina, Y. Grincourt, I.J. Davidson, Y.C. Yoo, D.Y. Seung, *J. Power Sources*, 97-98 (2001) 541.
13. B.L. Ellis, K.T. Lee, L.F. Nazar, *Chem. Mater*., 22 (2010) 691.
14. J.S. Kim, C.S. Johnson, J.T. Vaughey, M.M. Thackeray, *J. Power Sources*, 153 (2006) 258.
15. H. Deng, I. Belharouak, R.E. Cook, H. Wu, Y.K. Sun, K, Amine, *J. Electrochem. Soc*., 157 (2010) A447.
16. Y. Sun, Y. Shiosaki, Y. Xia, H. Noguchi, *J. Power Sources*, 159 (2006) 1353.
17. J.M. Zheng, X.B. Wu, Y. Yang, *Electrochim. Acta*, 56 (2011) 3071.
18. A. Ito, D. Li, Y. Ohsawa, Y. Sato, *J. Power Sources*, 183 (2008) 344.
19. D.H. Kim, J.H. Gim, J.S. Lim, S.J. Park, J.K. Kim, *Mater. Res. Bull*., 45 (2010) 252.
20. S.H. Park, C.S. Yoon, S.G. Kang, H.S. Kim, S.I. Moon, Y.K. Sun, *Electrochim. Acta*, 49 (2004) 557.
21. S.H. Park, S.H. Kang, I. Belharouak, Y.K. Sun, K. Amine, *J. Power Sources*, 177 (2008) 177.
22. C.S. Johnson, N. Li, J.T. Vaughey, S.A. Hackney, M.M. Thackeray, *Electrochem. Commun*., 7 (2005) 528.
23. T. Takada, H. Hayakawa, E. Akiba, F. Izumi, B.C. Chakoumakos, *J. Power Sources*, 68 (1997) 613.
24. M.M. Thackeray, M.F. Mansuetto, C.S. Johnson, *J. Solid State Chem*., 125 (1996) 274.
25. Y.J. Shin, A. Manthiram, *Electrochim. Acta*, 48 (2003) 3583.
26. S.H. Ju, H.C. Jang, Y.C. Kang, *Electrochim. Acta*, 52 (2007) 7286.
27. I. Taniguchi, C.K. Lim, D. Song, M. Wakihara, *Solid State Ionics*, 146 (2002) 239.
28. Y.N. Ko, H.Y. Koo, J.H. Kim, J.H. Yi, Y.C. Kang, J.H. Lee, *J. Power Sources*, 196 (2011) 6682.
29. I. Taniguchi, D. Song, M. Wakihara, *J. Power Sources*, 109 (2002) 333.
30. Y.N. Ko, J.H. Kim, Y.J. Hong, Y.C. Kang, *Mater. Chem. Phys*., 131 (2011) 292.
31. K. Matsuda, I. Taniguchi, *J. Power Sources*, 132 (2004) 156.
32. X.C. Tang, B.Y. Huang, Y.H. He, *Trans. Nonferrous Met. Soc. China*, 16 (2006) 438.
33. S.H. Park, Y. Sato, J.K. Kim, Y.S. Lee, *Mater. Chem. Phys*., 102 (2007) 225.